

# Accurate energy bands calculated by the hybrid quasiparticle self-consistent $GW$ method implemented in the `ecalj` package

Daiki Deguchi and Kazunori Sato

*Division of Materials and Manufacturing Science, Graduate School of Engineering,  
Osaka University, 2-1 Yamadaoka, Suita, Osaka 565-0871, Japan*

Hiori Kino

*National Institute for Materials Science, Sengen 1-2-1, Tsukuba, Ibaraki 305-0047, Japan*

Takao Kotani

*Department of Applied Mathematics and Physics, Tottori University, Tottori 680-8552, Japan*

We have recently implemented a new version of the quasiparticle self-consistent  $GW$  (QSGW) method in the `ecalj` package released at <http://github.com/tkotani/ecalj>. Since the new version of the `ecalj` is numerically stable and more accurate compared to the previous versions, we can perform calculations easily without being bothered with setting input parameters. Here we examine its ability to describe energy band properties, *e.g.*, band-gap energy, eigenvalues at special points and effective mass, for variety of semiconductors and insulators. We treat C, Si, Ge, Sn, SiC (in 2H, 3C and 4H structures), (Al, Ga, In) $\times$ (N, P, As, Sb), (Zn, Cd, Mg) $\times$ (O, S, Se, Te), SiO<sub>2</sub>, HfO<sub>2</sub>, ZrO<sub>2</sub>, SrTiO<sub>3</sub>, PbS, PbTe, MnO, NiO and HgO. We propose that a hybrid QSGW method, where we mix 80 percent of QSGW and 20 percent of LDA, gives universally good agreement with experiments for these materials.

PACS numbers: 71.15.Ap, 71.20.Nr, 31.15.xm

## I. INTRODUCTION

The quasiparticle self-consistent  $GW$  method (QSGW) is the best available method to find out a static one-body Hamiltonian  $H^0$  which describes the system based on the optimum independent-particle (or the quasiparticle (QP)) picture [1–7]. QSGW looks for an optimum division of the full many-body Hamiltonian  $H$  into  $H = H^0 + (H - H^0)$ , by choosing  $H^0$  so as to minimize the perturbative corrections caused by  $(H - H^0)$  to the QPs described by  $H^0$ . That is, we perform a self-consistent calculation until the correction is minimized. Note that  $(H - H^0)$  should contain not only the bare Coulomb interaction but also quadratic term, which is missing in usual model Hamiltonians. In QSGW we evaluate  $(H - H^0)$  in the  $GW$  approximation, therefore, in the determination of  $H^0$ , charge fluctuations (not only local fluctuations but also plasmons) are taken into account self-consistently within the random phase approximation (RPA). We determine  $H^0$ , the self-energy  $\Sigma(\mathbf{r}, \mathbf{r}', \omega)$ , and the effective screened Coulomb interaction  $W(\mathbf{r}, \mathbf{r}', \omega)$  simultaneously when we attain the self-consistency in QSGW.

Kotani and his collaborators had developed an all-electron  $GW$  method based on the full-potential linear muffin-tin orbital (FPLMTO) method [8] to perform the QSGW calculations [1, 3]. We call this method FPLMTO-QSGW. The FPLMTO-QSGW was applied to a wide-range of materials and proved its potential to go beyond the abilities of current first-principles methods based on the density functional theory. [3, 7]. However, mainly because of the difficulty of the usage of FPLMTO, it is too complicated to apply FPLMTO-QSGW to wide

variety of materials. Main reason is that FPLMTO uses only the atom-centered localized orbitals, the Muffin-tin orbitals (MTOs), as a basis set to expand eigenfunctions. Choosing parameters specifying MTOs is not straightforward and requires fine tunings and repeated tests to perform reliable calculations. In addition, the offset-Gamma method to perform the Brillouin zone (BZ) integration is a little problematic to treat anisotropic systems.

To avoid these problems, Kotani and coworkers have developed a new implementation of the QSGW method based on the PMT method, that employs augmented plane wave (APW) and MTO basis set [5, 9]. The PMT method is a unique mixed basis method which uses two kinds of augmented waves [9–11]. We call this new implementation of QSGW as the PMT-QSGW and the package is open for public use as `ecalj` package which is available from <https://github.com/tkotani/ecalj/> [12]. In this paper, we present practical applications of the PMT-QSGW with `ecalj` to variety of materials. The present calculation results have not presented yet, although the PMT-QSGW with `ecalj` was already used in the preceding papers [13–18] and minimum examination of the PMT-QSGW was reported in Ref.[5]

The purpose of the present paper is twofold. On the one hand, we show how accurately the PMT-QSGW describes band structure of semiconductors and insulators. The first-principles calculations based on the local density approximation (LDA) are now frequently used for explaining material properties, but due to its deficiency in the prediction of band properties, such as energy gap and effective mass, the application range is somewhat limited. Obviously, we cannot directly use the LDA for proposing new photovoltaic or photocatalytic materials. Con-

sidering that the computational method becomes more and more important for exploring and fabricating new functional materials, it is quite important to show the reliability of the most advanced electronic structure theory, so-called ‘beyond LDA’ theory such as QSGW, and encourage the first-principles calculations as a standard tool for designing new functional materials.

The other purpose of the present paper is to demonstrate the usability of `ecalj`. Recently, the first-principles calculations are not limited only for theoretical researchers but used by experimentalists for practical applications. In such case, all users of the first-principles package are not always professionals. The `ecalj` is designed so that all the calculations are performed essentially in its default settings, therefore, the users are not bothered with the settings for parameters which controls the accuracy of the calculations. We just need to prepare the information of crystal structures with very limited number of inputs. By following the procedure described in the Appendix, the users of `ecalj` can reproduce the results presented in this paper and actually see the numerical stability and the reliability of `ecalj`, thus the present paper gives a reference of standard calculation results.

After minimum explanation of the PMT-QSGW in the next section, we show calculated band gaps. Then we show band properties and effective mass for materials of zincblende structures. Finally, we give a summary and possible expectations for the PMT-QSGW in `ecalj`. We would conclude that the PMT-QSGW in `ecalj` can be a useful tool to investigate problems not treated within the other standard electronic structure theories such as LDA and the hybrid methods. In the Appendix, we give how to reproduce our results with the `ecalj` package.

## II. METHOD

In this paper, we apply the QSGW method implemented in the `ecalj` package to several materials. Readers are referred to Ref.[5] for details on the theory and implementation of the QSGW method. In this section, we give a minimum explanation of the QSGW method.

In the LDA, we use  $V_{\text{LDA}}^{\text{xc}}(\mathbf{r})$  calculated from the electron density. This is calculated from a one-body Hamiltonian  $H^0$ . In contrast, we calculate  $\Sigma(\mathbf{r}, \mathbf{r}', \omega)$  from eigenfunctions and eigenvalues calculated from  $H^0$ . Then we can obtain static but non-local exchange-correlation potential in QSGW  $V_{\text{QSGW}}^{\text{xc}}(\mathbf{r}, \mathbf{r}')$ , whose matrix elements are given as

$$V_{\text{QSGW}}^{\text{xc}} = \frac{1}{2} \sum_{ij} |\psi_i\rangle \{ \text{Re}[\Sigma(\varepsilon_i)]_{ij} + \text{Re}[\Sigma(\varepsilon_j)]_{ij} \} \langle \psi_j|, \quad (1)$$

where  $\varepsilon_i$  and  $|\psi_i\rangle$  refer to the eigenvalues and eigenfunctions of  $H_0$ , respectively, and  $\Sigma_{ij}(\omega) = \langle \psi_i | \Sigma(\omega) | \psi_j \rangle = \int d^3r \int d^3r' \psi_i^*(\mathbf{r}) \Sigma(\mathbf{r}, \mathbf{r}', \omega) \psi_j(\mathbf{r}')$ .  $\text{Re}[\Sigma(\varepsilon)]$  is the real

part of the self-energy, which assure Hermiteness of the Hamiltonian [1, 3]. With this  $V_{\text{QSGW}}^{\text{xc}}$ , we can give a new static one-body Hamiltonian  $H^0$  (with keeping  $V_{\text{QSGW}}^{\text{xc}}$  instead of using  $V_{\text{LDA}}^{\text{xc}}(\mathbf{r})$ , we run a self-consistent calculation). Thus we can repeat the above procedure again and again, until  $H^0$  is converged. Simple semiconductors require about five iterations to achieve convergence of eigenvalues within  $\lesssim 0.01$  eV. More iteration are required for materials such as anti-ferromagnetic NiO and MnO. We should emphasize that the importance of off-diagonal elements of Eq. (1) to resolve band entanglement, *e.g.*, in Ge [36]. In such case, even for simple semiconductors as Ge, we need fifteen iterations to have well converged band-gap energy.

Generally speaking, the QSGW method systematically overestimates band-gap energy [2, 3]. As suggested in Ref.[2], this can be due to the too small screening effect in the RPA which neglect electron-hole correlations in the proper polarization function [4], and/or the screening effect of phonons suggested by Botti and Marques [37]. To remedy this problem empirically, we use a hybrid QSGW method [38]. In this paper, we use

$$V^{\text{xc}} = (1 - \alpha)V_{\text{QSGW}}^{\text{xc}} + \alpha V_{\text{LDA}}^{\text{xc}}, \quad (2)$$

where we assume  $\alpha = 0.2$ , that is, 80% QSGW plus 20 % LDA in the calculations presented here. We refer this QSGW80 in Sec. III, where we will see that QSGW80 works reasonably well for wide range of materials. This QSGW80 can be a simple solution to treat interfaces or superlattices such as CdSe/CdS [39], as long as both of materials are described well with the same  $\alpha$ .

The spin-orbit coupling (SO) is essential to obtain correct prediction of effective mass and band gap energy. Considering smallness of the effects of SO to systems treated here, we can include it as a perturbation after the self-consistency is attained.

## III. RESULTS

We calculate materials shown in the Table I. Their crystal structures and lattice constants are taken from experimental values. Not only fundamental IV, III-V and II-VI semiconductors, we include some important materials such as polytypes of SiC, Mg compounds, Pb compounds and some oxides such as cubic SiO<sub>2</sub>, HfO<sub>2</sub> and so on. We assume paramagnetic states except MnO and NiO which are in type II anti-ferromagnetic order [21]. For some materials such as AlN, we treat two structures, both of zincblende (ZB) and wurtzite (WZ) structures.

As shown in Table I, the number of  $\mathbf{k}$  points in the 1st Brillouin zone (BZ) for the calculations of self-energy are  $6 \times 6 \times 6$  for zincblende structure in which two atoms are in the primitive cell. For the other structures, we reduce the number so as to keep the number of  $\mathbf{k}$  points per atom is almost the same, *e.g.*, we use  $6 \times 6 \times 3$  for wurtzite structure.

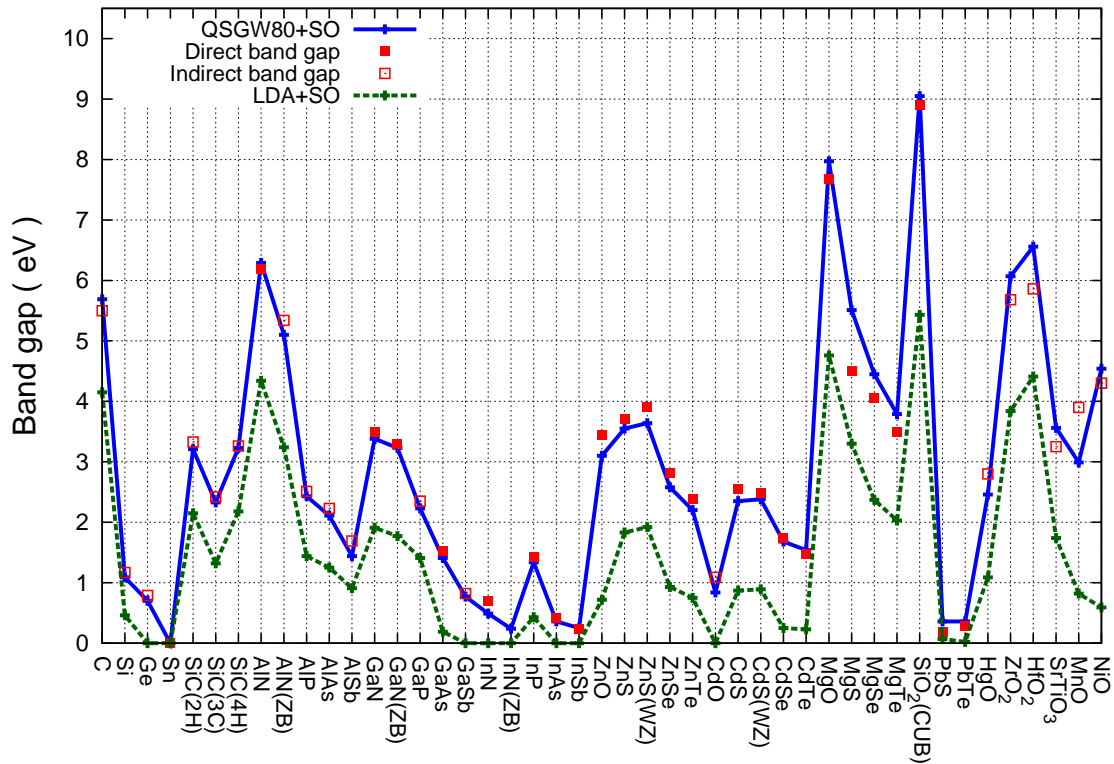


FIG. 1: Calculated band gap energy by using the QSGW80+SO (blue solid line) and the LDA+SO (green dotted line), together with the experimental values (solid squares: direct band gap, open squares: indirect band gap). Respective values are shown in Table II.

In `ecalj`, we use an interpolation technique for  $V_{\text{QSGW}}^{\text{xc}}$  in the whole BZ [5]. This interpolation allows us to use large number of  $\mathbf{k}$  points in the step to determine  $H^0$  for given  $V_{\text{QSGW}}^{\text{xc}}$ .  $V_{\text{QSGW}}^{\text{xc}}$  is calculated for the number of  $\mathbf{k}$  points shown in Table I.

Based on the convergence check as shown in Ref.[5], we guess that numerical errors can be  $\sim 0.1$  eV due to the settings of parameters in the calculations. The number of MTOs per atom were  $\sim 30$ , and it depends on atomic species. The cutoff energy of APW's is  $3 \text{ Ry} = 40.8 \text{ eV}$ , which is good enough to reproduce energy bands without empty spheres [5].

### A. Minimum band gap

Calculated minimum band-gap energies are shown in Table II. The label “+SO” means that the spin-orbit coupling was added after the convergence of QSGW iteration. The label “QSGW80” means the hybrid calculations with  $\alpha = 0.2$  in Eq. (2), that is, 80 % of QSGW plus 20 % of LDA. We see that the normal QSGW with SO, *i.e.* QSGW+SO, systematically overestimates band gap energy in comparison with experimental values. This overestimation was already observed in FPLMTO-QSGW [2, 3]. In contrast, we see that the QSGW80+SO

shows much better agreements with experiments systematically. In Fig. 1, we plot QSGW80+SO values given in Table II, together with experimental values.

For the most of semiconductors shown in Table II, the deviations of the theoretical predictions from the experimental values are as large as  $\sim 0.1$  eV. This is in the range of numerical uncertainty of our implementation. In some cases, error can be a little larger. For example, the calculated energy gap of InN(WZ) is 0.49 eV which is 0.21 eV smaller than the experimental value 0.7 eV. As for ZnO, calculated value of 3.44 eV is 0.34 eV away from the experimental one of 3.10 eV. This is a case that the calculated band gap is largely affected by  $\alpha$  since the LDA value is too small. For practical application to semiconductors, we need to take into consideration the accuracy revealed in the Table II. On the other hand, we have to note that experimental error bar of band gap of materials (especially oxides) may be not so small enough, for example, energy gap of MnO is  $3.9 \pm 0.4$  eV.

In QSGW80(NoSC)+SO, we use Eq. (2) after we get self-consistent  $V_{\text{QSGW}}^{\text{xc}}$  with  $\alpha = 0$  (usual QSGW). The difference from QSGW80+SO is not so large except for the cases such as NiO, where QSGW80(NoSC)+SO gives 5.00 eV on the other hand QSGW80+SO gives 4.54 eV. This difference is due to the localized 3d electrons on cation sites. One may think that the large difference

comes from existence of the localized 3d orbital near Fermi level, but it isn't true because they are 3.56 and 3.54eV for SrTiO<sub>3</sub>, the electric state of which is close to that of NiO apart from its magnetic nature. We can't discuss it further because we don't have enough data to investigate its origin. We see smaller but a little difference even in ZnO (3.10 and 3.26 eV).

We can see the size of the effect of SO as the difference between, *e.g.*, QSGW and QSGW+SO. As we see, materials including heavier atoms (especially as anion) show larger SO effects. The difference between QSGW and QSGW+SO is very similar to the difference between QSGW80 and QSGW80+SO. This justifies our perturbative procedure for the SO.

The label "QSGW1shot" means that the 1shot *GW* calculation from the LDA result and the diagonalization with including off-diagonal elements of  $V_{\text{QSGW}}^{\text{xc}}$  in Eq. (1). Thus we can solve the entanglement problem. This is why our calculation gives the band gap for Ge, where the usual one-shot *GW* (eigenvalue-shift only) cannot give the band gap [36]. In cases, QSGW1shot can be useful from the view of computational speed. The QSGW1shot can be used as a practical tool since it can give reasonable agreements with experiments for many semiconductors (To compare values with experiments, we need to add SO effect which can be taken as the difference between QSGW80 and QSGW80+SO), although it is not applicable to materials such as NiO.

## B. Band property of ZB-type semiconductors

The quasi-particle energies at specific  $\mathbf{k}$  points in BZ are key quantities in cases. For example, when we observe optical responses which contain both of direct and indirect transitions, or when we need to consider intervalley transitions. Here we show these eigenvalues instead of showing band plots (See Appendix about how to show band plots).

In Table III, we show the eigenvalues, which can be interpreted as quasi-particle energies, at the  $\Gamma$ ,  $X$ ,  $L$  points for five selected ZB materials. These values can be compared with those calculated in the hybrid functional HSE06 [40–42]. We can say QSGW80+SO shows good agreements with experiments. However, we also see its limitations of accuracy. For example,  $L_6^c$  and  $\Gamma_6^c$  for InP by QSGW80+SO are 2.18 and 1.34 eV, respectively. They are a little different from the experimental value 2.01 ( $L_6^c$ ) and 1.42 ( $\Gamma_6^c$ ) eV. The difference is a little larger than the agreement of band gap itself (1.34 eV (QSGW80+SO) and 1.42 eV (experiment) at  $\Gamma$  point). Thus we need to be careful about this level of errors when we apply QSGW80+SO to materials. However, we simultaneously need to note accuracy of experimental data shown in Table III. These are mostly estimated by optical experiments, where we "undo" excitonic effects from the raw experimental data based on some simple assumptions. Therefore, the difference between QSGW80+SO

and HSE06 could be within the experimental errors.

HSE06 values, taken from Ref.[40], also give good agreements with experiments. The HSE06 uses GGA, but corrects a short-range exchange part with the Hartree-Fock exchange term. Since the Hartree-Fock method can give very large band gaps, results can be strongly affected by the hybridization ratio. This is in contrast to the QSGW80 that we just hybridized 20 % of LDA so as to correct small error of QSGW. One interesting observation is that HSE06 and QSGW80+SO gives similar tendency as for differences from experimental values. For example, the valence band width  $X_7^v$  of InP are -2.49 and -2.52 eV for QSGW80+SO and HSE06, respectively.

## C. Effective mass of ZB-type semiconductors

Effective mass plays a key role when we evaluate transport properties and eigenvalues in quantum well structures and so on. It is straightforward to calculate effective mass in QSGW in `ecalj` since we have interpolation procedure in the whole BZ, namely without any extra techniques such as the Wannier interpolation we can plot band structure. We show the calculated effective mass along [100] direction for ZB in Table IV (the effective mass along other directions are complicated [38]). As discussed in Ref.[40], improvement of the prediction of band gap energy is essential in the correct prediction of the effective mass. As we see in Table IV, the agreement with experiments are rather satisfactory, especially for the electron mass. If we like to treat subband structure of superlattice such as CdS/CdSe [39], we have to use a method which can reproduce not only the band gap and band offset, but also the effective mass. This is never expected by methods such as the LDA nor by the constant-shift procedure of band gap (scissors operator procedure). In this sense, careful treatment may be necessary to compare experimental data with the results in Ref.[39].

## IV. SUMMARY

We have examined the ability for the QSGW method and the hybrid method QSGW80 implemented in the `ecalj` package as a tool for predicting band properties such as band gap energy, eigenvalues at special points and the effective mass. The `ecalj` package can be used easily since the setting of parameters for calculations are automatically chosen. With the hybrid scheme QSGW80, we can expect that the accuracy of band gaps can be  $\sim 0.1$  eV for usual semiconductors. This level of accuracy is much better than what we expect in the LDA. Considering the fact that QSGW can treat even metals accurately [3, 14, 15], we can expect that the QSGW or the "hybrid QSGW" method can be applicable to complex systems such as metal/semiconductor interfaces. However, it is

necessary to know its limitations shown in this paper for such applications.

### Acknowledgments

This work was partly supported by Advanced Low Carbon Technology Research and Development Program (ALCA) of Japan Science and Technology Agency (JST), and by Grant-in-Aid for Scientific Research 23104510 and 26286074. We also acknowledge computing time provided by Computing System for Research in Kyushu University.

### Appendix A: How to reproduce the calculations in this paper by the `ecalj` package

The `ecalj` package is open for public use and all of the results presented in this paper can be reproduced by using the `ecalj` by yourself. In this Appendix, calculation procedure is briefly explained step by step. Due to the limitation of space, we can show only the outline of the procedure. For detailed explanations and descriptions, visit <https://github.com/tkotani/ecalj>[12].

- 1. Installation of `ecalj`:** `ecalj` can be downloaded and installed from Ref.[12]. The installer generates required binaries by using Fortran compiler and performs minimum test calculations successively.
- 2. Preparation of `ctrls.*` file:** To start a calculation of target material, we need to prepare a `ctrls.*` file, which contains the information of crystal structure. For the extension `*`, we usually use the name of the material, such as `gaas`, `zno` and so on. Detailed description of `ctrls` file is explained at the link[12]. Instead of making `ctrls.*` by hand, you can use a converter, for example, `vasp2ctrl` is prepared for extracting the information of crystal structure from POSCAR file for VASP (concerning to VASP, see <https://www.vasp.at/>).
- 3. Generating `ctrl` file:** From the `ctrls.*`, next we generate a `ctrl.*` file by using a python script, `ctrlgenM1.py` included in the `ecalj` package. In addition to the information of the crystal structure, `ctrl.*` contains all of the parameters which control the calculations, such as the information on MTO's, the xc-potential, number of k-points, relativistic treatment, and so on. In the generated `ctrl.*`, default settings are set to guarantee a reasonable calculation, but we need to edit it depending on the necessity. (With `ctrl.*` we can perform DFT calculations.)
- 4. Generating `GWinput`:** In addition to `ctrl` file, we need one more input file, `GWinput`, which can

be generated from `ctrls.*` by using a shell script (`mkGWIN_lmf2` also included in the `ecalj` package). `GWinput` contains settings for GW calculation.

The input files used in this paper are basically produced from the `ctrls.*` by following the above processes (2)-(4). To facilitate the reproduction of the present calculations by the users, we packed `ctrls.*`, `ctrl.*` and `GWinput` for each material, and they are available as supplementary data of this article at the web page[43].

- 5. Performing QSGW:** With the two input files `ctrl.*` and `GWinput`, we can perform QSGW calculations by using a script `gwsc`. We set number of iterations when we submit a job of `gwsc`. The output files of QSGW calculations are stored in `rst.*` and `sigm.*`. The outputs for the materials treated in this paper can be found also at the web page[43]. After we check convergence of eigenvalues, we go ahead to do post-processing such as energy bands plot.
- 6. Post processing:** Once the self-consistency is obtained, we can extract any material properties from the calculated electronic structure. But how to do it is not trivial and additional calculations or post-processing is needed. As concerned with this paper, it is necessary to plot and fit energy bands for estimating effective mass. As an example, the energy bands of CdO is shown in Fig. 2 The energy-band plots for the other materials and fitting results can be found at the web page[43]. The files `syml.*`, which describes the kpoint path for band structure plot, are also packed. More details concerning to the band plot can be found in the README given in the page[43].

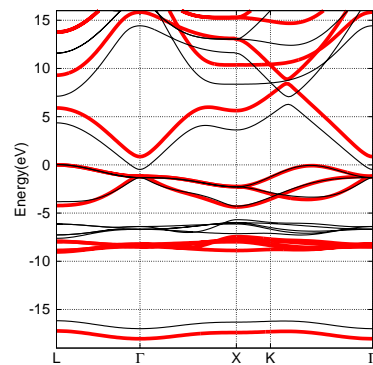


FIG. 2: Calculated band structure of CdO by using the LDA (thin black lines) and by using the QSGW80 (thick red lines). The energy is relative to the valence band maximum.

- 
- [1] S. Faleev, M. van Schilfgaarde and T. Kotani, Phys. Rev. Lett. **93**, 126406 (2004).
- [2] M. van Schilfgaarde, T. Kotani and S. Faleev, Phys. Rev. Lett. **96**, 226402 (2006).
- [3] T. Kotani and M. van Schilfgaarde, Phys. Rev. B **76**, 165106 (2007).
- [4] M. Shishkin, M. Marsman and G. Kresse, Phys. Rev. Lett. **99**, 246403 (2007).
- [5] T. Kotani, J. Phys. Soc. Jpn. **83**, 094711 (2014).
- [6] J. Klimeš, M. Kaltak and G. Kresse, Phys. Rev. B **90**, 075125 (2014).
- [7] F. Bruneval and M. Gatti, *First Principles Approaches to Spectroscopic Properties of Complex Materials*, Eds. C. Di Valentin, S. Botti and M. Cococcioni (Springer Berlin Heidelberg, Berlin, Heidelberg, 2014) Vol. 347, p. 99.
- [8] M. Methfessel, M. v. Schilfgaarde and R. A. Casali, *Electronic Structure and Physical Properties of Solids: The Uses of the LMTO Method, Lecture Notes in Physics*, ed. H. Dreyse (Springer-Verlag, Berlin, 2000) Vol. 535.
- [9] T. Kotani, H. Kino and H. Akai, J. Phys. Soc. Jpn. **84**, 034702 (2015).
- [10] T. Kotani and M. van Schilfgaarde, Phys. Rev. B **81**, 125117 (2010).
- [11] T. Kotani and H. Kino, J. Phys. Soc. Jpn. **82**, 124714 (2013).
- [12] A first-principles electronic-structure suite based on the PMT method, `ecalj` package, is freely available from <https://github.com/tkotani/ecalj>. Its one-body part is developed based on the LMTO part in the LMSuit package at <http://www.lmsuite.org/>.
- [13] H. Ryee, S. Jang, H. Kino, T. Kotani and M. Han, arXiv:1507.08746.
- [14] S. W. Jang, T. Kotani, H. Kino, K. Kuroki and M. J. Han, Sci. Rep. **5**, 12050 (2015).
- [15] M. J. Han, H. Kino and T. Kotani, Phys. Rev. B **90**, 035127 (2014).
- [16] H. Nagara, T. Ishikawa and T. Kotani, High Pressure Res. **34**, 215 (2014).
- [17] M. Geshi and T. Fukazawa, Physica B **411**, 154 (2013).
- [18] A. Bakhtatou and A. Meddour, Phys. Status Solidi B [doi: 10.1002/pssb.201552490].
- [19] Crystallography Open Database (COD). URL <http://www.crystallography.net>
- [20] P. Mélinon, *SiC cage like based materials* (INTECH Open Access Publisher, 2011).
- [21] K. Terakura, T. Oguchi, A. R. Williams and J. Kübler, Phys. Rev. B **30**, 4734 (1984).
- [22] L. W. S. H. Vosko and M. Nusair, Can. J. Phys. **58**, 1200 (1980).
- [23] *Springer handbook of condensed matter and materials data*, Eds. W. Martienssen and H. Warlimont (Springer, New York, 2005).
- [24] W. J. Choyke, D. R. Hamilton and L. Patrick, Phys. Rev. **133**, A1163 (1964).
- [25] M. P. Thompson, G. W. Auner, T. S. Zheleva, K. A. Jones, S. J. Simko and J. N. Hilfiker, J. Appl. Phys. **89**, 3331 (2001).
- [26] G. Ramírez-Flores, H. Navarro-Contreras, A. Lastras-Martínez, R. C. Powell and J. E. Greene, Phys. Rev. B **50**, 8433 (1994).
- [27] V. Davydov, A. A. Klochikhin, R. P. Seisyan, V. V. Emtsev, S. V. Ivanov, F. Bechstedt, J. Furthmüller, H. Harima, A. V. Mudryi, J. Aderhold, O. Semchinova and J. Graul, Phys. Status Solidi B **229**, R1 (2002).
- [28] V. Davydov, A. A. Klochikhin, V. V. Emtsev, S. V. Ivanov, V. V. Vekshin, F. Bechstedt, J. Furthmüller, H. Harima, A. V. Mudryi, A. Hashimoto, A. Yamamoto, J. Aderhold, J. Graul and E. E. Haller, Phys. Status Solidi B **230**, R4 (2002).
- [29] O. Zakharov, A. Rubio, X. Blase, M. L. Cohen and S. G. Louie, Phys. Rev. B **50**, 10780 (1994).
- [30] S.-H. Wei and A. Zunger, Phys. Rev. B **55**, 13605 (1997).
- [31] T. DiStefano and D. Eastman, Solid State Commun. **9**, 2259 (1971).
- [32] S. Sayan, R. A. Bartynski, X. Zhao, E. P. Gusev, D. Vanderbilt, M. Croft, H. M. Banaszak-Holl and E. Garfunkel, Phys. Status Solidi B **241**, 2246 (2004).
- [33] S. Sayan, T. Emge, E. Garfunkel, X. Zhao, L. Wielunski, R. A. Bartynski, D. Vanderbilt, J. S. Suehle, S. Suzer and M. Banaszak-Holl, J. Appl. Phys. **96**, 7485 (2004).
- [34] K. van Benthem, C. Elsässer and R. H. French, J. Appl. Phys. **90**, 6156 (2001).
- [35] F. Tran and P. Blaha, Phys. Rev. Lett. **102**, 226401 (2009).
- [36] M. van Schilfgaarde, T. Kotani and S. Faleev, Phys. Rev. B **74**, 245125 (2006).
- [37] S. Botti and M. A. L. Marques, Phys. Rev. Lett. **110**, 226404 (2013).
- [38] A. N. Chantis, M. van Schilfgaarde and T. Kotani, Phys. Rev. Lett. **96**, 086405 (2006).
- [39] V. Kocevski, J. Ruzs, O. Eriksson and D. Sarma, Sci. Rep. **5**, 10865 (2015).
- [40] Y.-S. Kim, M. Marsman, G. Kresse, F. Tran and P. Blaha, Phys. Rev. B **82**, 205212 (2010).
- [41] J. Heyd, G. E. Scuseria and M. Ernzerhof, J. Chem. Phys. **118**, 8207 (2003).
- [42] J. Heyd, G. E. Scuseria and M. Ernzerhof, J. Chem. Phys. **124**, 219906 (2006).
- [43] Supplemental information is given at <https://github.com/tkotani/Supplement4deguchipaper.git>. It contains all informations to perform calculations presented in this paper. Output files of QSGW calculations are also available with the band-structure plots and the fitting results for effective mass calculations.

TABLE I: Crystal structures used for the calculations in this paper and the number of  $\mathbf{k}$  points for the self-energy calculations in the 1st Brillouin zone (see text). Labels mean as follows; COD:the ID number of the crystal open database [19], DIA:Diamond structure, HEX:Hexagonal structure, ZB: Zinblende structure, WZ:Wurtzite structure, RS:Rocksalt structure, CUB:Cubic structure, MONO:Monoclinic structure, TETRA:Tetragonal structure, PERO:Perovskite structure.

	Lattice constants ( $\text{\AA}$ )	Crystal Structure	Number of $\mathbf{k}$ for $\Sigma$
C	$a = 3.567$	DIA	$6 \times 6 \times 6$
Si	$a = 5.431$	DIA	$6 \times 6 \times 6$
Ge	$a = 5.646$	DIA	$6 \times 6 \times 6$
Sn	$a = 6.489$	DIA	$6 \times 6 \times 6$
SiC(2H)	$a = 3.076, c = 5.048$	HEX, COD9008875	$6 \times 6 \times 3$
SiC(3C)	$a = 4.348$	ZB, COD9008856	$6 \times 6 \times 6$
SiC(4H)	$a = 2.079, c = 10.07$	HEX, Ref.[20]	$4 \times 4 \times 2$
AlN(WZ)	$a = 3.112, c = 4.982$	WZ	$6 \times 6 \times 3$
AlN(ZB)	$a = 4.38$	ZB	$6 \times 6 \times 6$
AlP	$a = 5.467$	ZB	$6 \times 6 \times 6$
AlAs	$a = 5.661$	ZB	$6 \times 6 \times 6$
AlSb	$a = 6.136$	ZB	$6 \times 6 \times 6$
GaN(WZ)	$a = 3.189, c = 5.189$	WZ	$6 \times 6 \times 3$
GaN(ZB)	$a = 4.50$	ZB	$6 \times 6 \times 6$
GaP	$a = 5.451$	ZB	$6 \times 6 \times 6$
GaAs	$a = 5.653$	ZB	$6 \times 6 \times 6$
GaSb	$a = 6.096$	ZB	$6 \times 6 \times 6$
InN(WZ)	$a = 3.545, c = 5.703$	WZ	$6 \times 6 \times 3$
InN(ZB)	$a = 4.98$	ZB	$6 \times 6 \times 6$
InP	$a = 5.870$	ZB	$6 \times 6 \times 6$
InAs	$a = 6.058$	ZB	$6 \times 6 \times 6$
InSb	$a = 6.479$	ZB	$6 \times 6 \times 6$
ZnO	$a = 3.254$	WZ	$6 \times 6 \times 3$
ZnS(ZB)	$a = 5.413$	ZB	$6 \times 6 \times 6$
ZnS(WZ)	$a = 3.82, c = 6.26$	WZ	$6 \times 6 \times 3$
ZnSe	$a = 5.667$	ZB	$6 \times 6 \times 6$
ZnTe	$a = 6.101$	ZB	$6 \times 6 \times 6$
CdO	$a = 4.72$	RS	$6 \times 6 \times 6$
CdS(ZB)	$a = 5.826$	ZB	$6 \times 6 \times 6$
CdS(WZ)	$a = 4.160, c = 6.756$	WZ	$6 \times 6 \times 3$
CdSe	$a = 6.054$	ZB	$6 \times 6 \times 6$
CdTe	$a = 6.482$	ZB	$6 \times 6 \times 6$
MgO	$a = 4.212$	RS	$6 \times 6 \times 6$
MgS	$a = 5.62$	ZB	$6 \times 6 \times 6$
MgSe	$a = 5.91$	ZB	$6 \times 6 \times 6$
MgTe	$a = 6.42$	ZB	$6 \times 6 \times 6$
PbS	$a = 5.936$	RS	$6 \times 6 \times 6$
PbTe	$a = 6.462$	RS	$6 \times 6 \times 6$
SiO <sub>2c</sub>	$a = 7.165$	CUB	$4 \times 4 \times 4$
HgO	$a = 6.613, b = 5.521$ $c = 3.522$	MONO COD9012530	$2 \times 2 \times 4$
ZrO <sub>2</sub>	$a = 3.559, c = 5.111$	TETRA	$4 \times 4 \times 2$
HfO <sub>2</sub>	$a = 3.545, c = 5.102$	TETRA	$4 \times 4 \times 2$
SrTiO <sub>3</sub>	$a = 3.90$	PERO	$4 \times 4 \times 4$
MnO	$a = 4.445$	RS,AF-II, Ref.[21]	$4 \times 4 \times 4$
NiO	$a = 4.170$	RS,AF-II, Ref.[21]	$4 \times 4 \times 4$

TABLE II: Calculated minimum band-gap energy in eV by several calculation procedures. “+SO” means that the spin-orbit interaction is included after the self-consistency. QSGW80 means calculations with 80 percent of QSGW together with 20 percent of LDA. QSGW80(NoSC) means we use Eq. (2) when we make band plot after the convergence of (pure) QSGW. QSGW1shot means one-shot QSGW (including offdiagonal elements) from the LDA. In the LDA, we use the VWN exchange-correlation functional [22]. Expt. means experimental values, and D/I distinguishes the direct or indirect band gap. Experimental values are taken from Ref.[23] otherwise indicated. QSGW80+SO values together with LDA+SO and experimental ones are plotted in Fig. 1.

	LDA	LDA	QSGW	QSGW	QSGW	QSGW80	QSGW80	QSGW80	Expt.	D/I
	+SO		+SO		1shot	+SO		(NoSC)+SO		
C	4.16	4.15	6.11	6.11	5.88	5.69	5.69	5.71	5.50	I
Si	0.47	0.46	1.28	1.26	1.20	1.10	1.09	1.11	1.17	I
Ge	0.00	0.00	1.03	0.93	0.81	0.80	0.70	0.74	0.79	I
Sn	0.00	0.00	0.12	0.00	0.00	0.00	0.00	0.00	0	D
SiC(2H)	2.16	2.15	3.56	3.51	3.35	3.21	3.21	3.24	3.33	I
SiC(3C)	1.32	1.32	2.63	2.62	2.47	2.33	2.33	2.36	2.42	I
SiC(4H)	2.18	2.18	3.53	3.53	3.35	3.23	3.23	3.98	3.26[24]	I
AlN	4.34	4.34	6.91	6.91	6.41	6.30	6.29	6.40	6.19	D
AlN(ZB)	3.24	3.24	5.67	5.67	5.23	5.10	5.10	5.19	5.34[25]	I
AlP	1.46	1.44	2.74	2.72	2.56	2.45	2.43	2.47	2.51	I
AlAs	1.35	1.25	2.46	2.36	2.29	2.20	2.11	2.17	2.23	I
AlSb	1.13	0.91	1.80	1.59	1.69	1.65	1.44	1.49	1.69	I
GaN	1.91	1.91	3.84	3.83	3.45	3.38	3.38	3.45	3.50	D
GaN(ZB)	1.77	1.77	3.69	3.68	3.30	3.24	3.23	3.30	3.30[26]	D
GaP	1.44	1.41	2.49	2.46	2.31	2.25	2.23	2.26	2.35	I
GaAs	0.30	0.19	1.89	1.77	1.58	1.52	1.41	1.46	1.52	D
GaSb	0.00	0.00	1.20	0.99	1.01	0.99	0.77	0.79	0.82	I
InN	0.00	0.00	0.80	0.80	0.27	0.49	0.49	0.61	0.7[27, 28]	D
InN(ZB)	0.00	0.00	0.55	0.55	0.18	0.24	0.24	0.38	—	D
InP	0.46	0.43	1.65	1.62	1.40	1.37	1.34	1.38	1.42	D
InAs	0.00	0.00	0.80	0.68	0.47	0.48	0.36	0.43	0.42	D
InSb	0.00	0.00	0.77	0.54	0.51	0.49	0.25	0.29	0.24	D
ZnO	0.74	0.72	3.88	3.87	2.91	3.10	3.10	3.26	3.44	D
ZnS	1.86	1.83	4.12	4.10	3.62	3.57	3.55	3.65	3.71	D
ZnS(WZ)	1.94	1.92	4.21	4.18	3.70	3.66	3.64	3.74	3.91[29]	D
ZnSe	1.06	0.93	3.23	3.10	2.73	2.71	2.58	2.68	2.82	D
ZnTe	1.03	0.75	2.92	2.64	2.54	2.48	2.20	2.28	2.39	D
CdO	0.00	0.00	1.32	1.32	0.53	0.85	0.84	0.98	1.09	I
CdS	0.89	0.87	2.86	2.84	2.34	2.37	2.35	2.45	2.55[29]	D
CdS(WZ)	0.91	0.89	2.90	2.88	2.36	2.40	2.38	2.48	2.48	D
CdSe	0.37	0.25	2.28	2.16	1.71	1.81	1.68	1.78	1.74	D
CdTe	0.52	0.23	2.24	1.97	1.80	1.81	1.54	1.63	1.48	D
MgO	4.77	4.76	8.97	8.96	8.22	7.98	7.97	8.14	7.67	D
MgS	3.33	3.30	6.23	6.20	5.63	5.54	5.51	5.63	4.5	D
MgSe	2.50	2.37	5.24	5.11	4.67	4.58	4.45	4.59	4.05	D
MgTe	2.31	2.03	4.50	4.24	4.13	4.05	3.79	3.90	3.49	D
PbS	0.26	0.07	0.73	0.49	0.63	0.62	0.36	0.39	0.19[30]	D
PbTe	0.67	0.02	1.06	0.47	0.99	0.98	0.36	0.38	0.29[30]	D
SiO2(CUB)	5.43	5.43	10.09	10.09	9.29	9.05	9.05	9.19	8.9[31]	D
HgO	1.11	1.09	2.89	2.89	2.53	2.49	2.46	2.54	2.8	I
ZrO2	3.84	3.84	6.83	6.83	6.12	6.07	6.07	6.11	5.68[32]	I
HfO2	4.42	4.41	7.29	7.25	6.63	6.57	6.56	6.61	5.86[33]	I
SrTiO3	1.75	1.74	4.26	4.25	2.17	3.58	3.56	3.54	3.25[34]	I
MnO	0.89	0.82	3.94	3.82	2.10	3.10	2.99	3.29	3.9[35]	I
NiO	0.59	0.59	5.59	5.59	2.16	5.29	4.54	5.00	4.3[35]	I



TABLE III: Eigenvalues (in eV) relative to the top of the valence band at  $\Gamma$  point for five selected zincblende materials. The values by HSE06 [40] include the spin-orbit coupling. Experimental values are also taken from Ref.[40].

Material	$E_g$	QSGW	QSGW80	HSE06	Expt.
		+SO	+SO		
InP	$\Gamma_6^c$	1.62	1.34	1.48	1.42
	$X_6^c$	2.48	2.26	2.35	2.38
	$X_7^v$	-2.54	-2.49	-2.52	-2.20
	$L_6^c$	2.46	2.18	2.25	2.01
	$L_{4,5}$	-1.05	-1.03	-1.03	-1.00
InAs	$\Gamma_6^c$	0.68	0.36	0.42	0.42
	$X_6^c$	2.09	1.88	1.98	1.90
	$X_7^v$	-2.65	-2.60	-2.64	-2.70
	$L_6^c$	1.74	1.46	1.53	—
	$L_{4,5}$	-1.07	-1.05	-1.06	-0.90
InSb	$\Gamma_6^c$	0.54	0.25	0.28	0.24
	$X_6^c$	1.55	1.41	1.53	1.80
	$X_7^v$	-2.62	-2.57	-2.66	-2.24
	$L_6^c$	1.00	0.79	0.85	0.93
	$L_{4,5}$	-1.11	-1.09	-1.12	-1.05
GaAs	$\Gamma_6^c$	1.77	1.41	1.33	1.52
	$X_6^c$	2.09	1.88	1.96	2.18
	$X_7^v$	-2.99	-2.93	-2.99	-2.80
	$L_6^c$	1.98	1.69	1.67	1.85
	$L_{4,5}$	-1.25	-1.23	-1.25	-1.30
GaSb	$\Gamma_6^c$	1.09	0.77	0.72	0.81
	$X_6^c$	1.19	1.05	1.26	1.14
	$X_7^v$	-2.90	-2.86	-2.95	-2.72
	$L_6^c$	0.99	0.78	0.87	0.88
	$L_{4,5}$	-1.67	-1.26	-1.29	-1.32

TABLE IV: Effective mass ( $m_e$ : electron,  $m_{lh}$ : light hole,  $m_{hh}$ : heavy hole, and  $m_{so}$ : split off band) along [100] direction calculated by QSGW80+SO. For the fitting region from 0.1eV to 0.5eV, we use a fitting formula  $E(1 + E/E_0) = k^2/2m$  to determine the effective mass. We have poor fitting for  $m_{lh}$  and  $m_{so}$  for GaN(ZB) and InN(ZB). Parentheses are experimental values taken from Ref.[40].

	$m_e$	$m_{lh}$	$m_{hh}$	$m_{so}$
GaAs	0.067 (0.067)	0.085 (0.090)	0.319 (0.350)	0.166 (0.172)
GaSb	0.043 (0.039)	0.049 (0.044)	0.231 (0.250)	0.142 (0.120)
GaN(ZB)	0.190	—	0.807	—
InP	0.080 (0.080)	0.103 (0.121)	0.411 (0.531)	0.174 (0.210)
InAs	0.027 (0.026)	0.033 (0.027)	0.346 (0.333)	0.106 (0.140)
InSb	0.019 (0.014)	0.021 (0.015)	0.254 (0.263)	0.129 (0.110)
InN(ZB)	0.035	—	1.027	—
ZnS	0.188	0.254	0.643	0.377
ZnSe	0.130	0.178	0.542	0.316
ZnTe	0.115	0.138	0.396	0.288
CdS	0.155	0.205	0.695	0.336
CdSe	0.108	0.148	0.578	0.292
CdTe	0.097	0.118	0.420	0.288
MgS	0.251	0.415	1.252	0.639
MgSe	0.203	0.332	1.038	0.558
MgTe	0.177	0.263	0.734	0.500